Thermal Strain in the Mushy Zone for Aluminum Alloys

AAGE STANGELAND, ASBJØRN MO, and DMITRY ESKIN

The parameters in a recently developed constitutive equation for macroscopic thermal strain in the mushy zone have been determined for the commercial alloys A356, AA2024, AA6061, and AA7075 in addition to an Al-4 wt pct Cu alloy. The constitutive equation for macroscopic thermal strain in the mushy zone reflects that there is no thermal strain in the solid part of the mushy zone at low solid fractions and that the thermal strain in the mushy zone approaches thermal strain in the fully solid material as the solid fraction increases toward 1. The development of thermal strain in the mushy zone is determined by combining experimentally measured contraction of a cast sample with thermomechanical simulations. Experiments were performed at cooling rates in the range from 2 to 5.5 °C/s. The solid fractions when the tested alloys start to contract, g_s^{th}, are in the range from 0.63 to 0.94. Grain refinement increases g_s^{th} for all the tested alloys. For most of the tested alloys the thermal strain in the mushy zone increases rapidly to the same level as thermal strain in fully solid material once the solid fraction becomes higher than g_s^{th}.

I. INTRODUCTION

HOT tearing is one of the major defects that can occur during solidification of alloys. This defect is believed to be a result of inadequate melt feeding that initiates tears and deformation, leading to the opening and propagation of the tears. This type of defect appears at the end of the solidification when the solid fraction is high.[1] Two main mechanisms associated with hot tearing are the solidification shrinkage leading to interdendritic melt flow[2] and the thermally induced deformation caused by nonuniform cooling contraction of the casting.[3,4]

A mathematical model addressing these phenomena (*i.e.,* shrinkage-driven melt flow and thermally induced deformation) in an isotropic mushy zone was recently proposed by Mo *et al*.[3,5] This model is based upon general volume-averaged conservation equations.[6] One challenge in such a modeling is to establish reliable constitutive relations for thermally induced deformations.

Thermal strain is the driving force for thermally induced deformations. While the thermal strain can easily be related to the density variation with temperature in a one-phase continuum, the situation is more complicated in the two-phase mushy zone (Figure 1). At low solid fractions, the bonds between the individual dendrites are relatively weak or even nonexistent. The dendrites can therefore contract with decreasing temperature without affecting the positions of their individual mass centers. Such solid-phase volume change would be accompanied by unlimited liquid feeding. Consequently there will be no thermal strain transmitted through the mushy zone—*i.e.,* there will be no macroscopic thermal strain imposed onto the mushy zone.* At high solid fractions, on the other hand, there is reason to believe that dendrites will coalesce or tangle,[7,8] meaning that a change in the solid density would be reflected in a nonzero macroscopic thermal strain as in the one-phase continuum. In this work, the critical solid fraction when the macroscopic thermal strain becomes nonzero is referred to as the solid fraction at onset of contraction, g_s^{th}.

*Macroscopic thermal strain rate is in this study the volume-averaged thermal strain rate calculated based on volume-averaged velocity gradients.

A constitutive equation for thermal strain in the mushy zone has recently been established,[9] and the parameters in this relation were determined for binary Al-Cu alloys. The purpose of the current study is to determine the parameters in the constitutive equation for thermal strain for the commercial aluminum alloys A356, AA2024, AA6061, and AA7075.

The experimental setup is presented in Section II, and modeling of thermal strain in the mushy zone is shown in Section III. The results showing how thermal strains can be related to the measurements are given in Section IV. The results are discussed in Section V.

II. EXPERIMENTAL PROCEDURE

The experimental procedure is identical to the method described in Reference 9, so only its main aspects are presented here. The experimental setup is based on the so-called linear solidification contraction experiment developed earlier and described in detail elsewhere[10,11,12] in which the contraction of the coherent mushy zone is measured and the solid fraction at which this contraction starts is calculated based on the measured temperature. The linear solidification contraction is here the change of linear dimensions in the horizontal plane of a cast sample during solidification. A schematic representation of the linear solidification contraction experiment[11,12] is shown in Figure 2. The casting mold is made of graphite, and the moving

AAGE STANGELAND, Scientist, formerly with SINTEF Materials and Chemistry, N-0314 Oslo, Norway, and the University of Oslo, N-0316, Oslo, Norway, is now with The Bellona Foundation, N-0505 Oslo, Norway. ASBJØRN MO, Professor, is with SINTEF Materials and Chemistry, N-0314 Oslo, Norway, and the University of Oslo, N-0316, Oslo, Norway. Contact e-mail: asbjorn.mo@sintef.no DMITRY ESKIN, Senior Scientist, is with the Netherlands Institute for Metals Research, 2628CD, Delft, The Netherlands.

Manuscript submitted February 23, 2005.

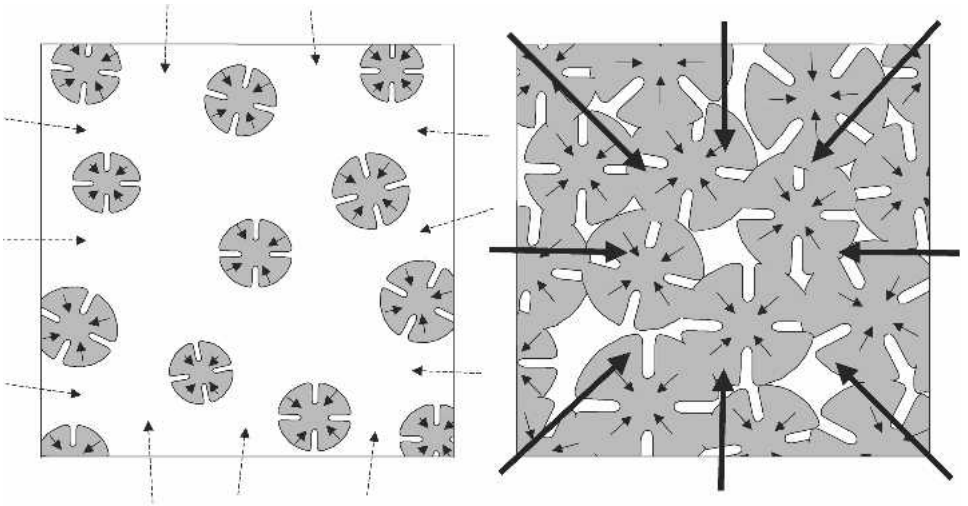

Fig. 1—Left: Thermal contraction of the dendrites in a two-phase volume element is accompanied by liquid melt feeding at low solid fractions. Right: Dendrites are coalesced together at high solid fractions and solid density change results in thermal strain. The small solid arrows indicate motion of the dendrites relative to their centers. The dashed arrows (left) indicate liquid flow into the volume element, and the bold solid arrows (right) indicate motion of volume-averaged solid phase into the volume element (*i.e.,* thermal strain). There will be no net flow of solid into the volume element in the left figure.

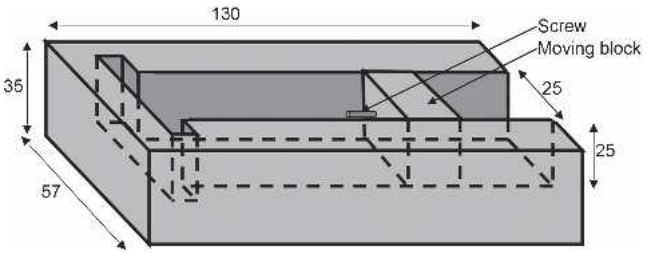

Fig. 2—Schematic view of the experimental setup. Dimensions are given in mm.

block to the right in the casting mold can slide in the cavity of the mold. During solidification the sample will be connected to the moving block when solidified material covers the screw that is initially fitted to the moving block.

The mold is initially at room temperature, and it is filled with a liquid aluminum alloy by gravity pouring from the top. During cooling of the alloy, solid coherent structures will first be formed at the bottom and walls near both the left and right ends of the mold[13] (Figure 3). As long as these two solid coherent structures are not directly connected to each other, there will be no displacement of the moving block because the contraction will be compensated by liquid feeding and the only manifestation of the shrinkage/contraction phenomenon is the decreasing melt level in the mold, as experimentally demonstrated elsewhere.[12] As the temperature decreases, the two solid coherent structures will grow toward the mold center and eventually coalesce to form one semisolid skeleton. This coherent structure will now be fixed to the left end of the casting mold due to the T-shape of the cavity. The coherent structure will also be connected to the moving block, as described previously. Further contraction will force the moving block in Figure 2 to move to the left. The displacement is measured by a linear displacement sensor connected to the moving block.

Due to gas evolution, the mushy zone will expand at high temperatures, when the sample is still in the slurry condition.[10,12] The temperature at the position of the arrow in Figure 3(b) at the instant when the displacement of the moving block shifts from expansion to contraction is defined as the temperature at onset of contraction, T^{th}. The solid fraction corresponding to T^{th} is called the solid fraction at onset of contraction, g_s^{th}, and it defines the local solid fraction corresponding to the formation of a continuous solid network that enables the transmission of thermal strain from one grain to another on the scale of the mushy zone (*i.e.,* the macroscopic thermal strain becomes nonzero).[9] The temperature at onset of contraction, T^{th}, is determined by extrapolating the temperature measured by thermocouple TC1 in Figure 3(b) to the position indicated by the arrow in Figure 3(b) based on the calculated temperature gradient between the surface point and TC1. The solid fraction at onset of contraction, g_s^{th}, is calculated based on T^{th}, and solid fractions as a function of temperature are, along with liquidus and solidus, based on data calculated by the Alstruc model.[14]

By defining the onset of contraction this way, T^{th} is actually the temperature when the expansion rate of the mushy zone equals the contraction rate of the mushy zone. However, the experimental measurements indicate that the expansion rate is very small at temperatures slightly above T^{th} compared to the contraction rate at temperatures slightly below T^{th}, which indicates that the expansion rate has only a small influence on T^{th}. The uncertainty in T^{th} due to the expansion of the mushy zone is believed to be negligible compared to the uncertainty in the calculated temperature gradient between the position of TC1 and the surface point indicated by the arrow in Figure 3(b).

Temperatures were measured by steel mantled thermocouples with an outer diameter of 0.5 mm and wire diameter of 0.1 mm. Two thermocouples were placed in the casting mold with positions as indicated in Figure 4. The thermocouples were calibrated against the melting points

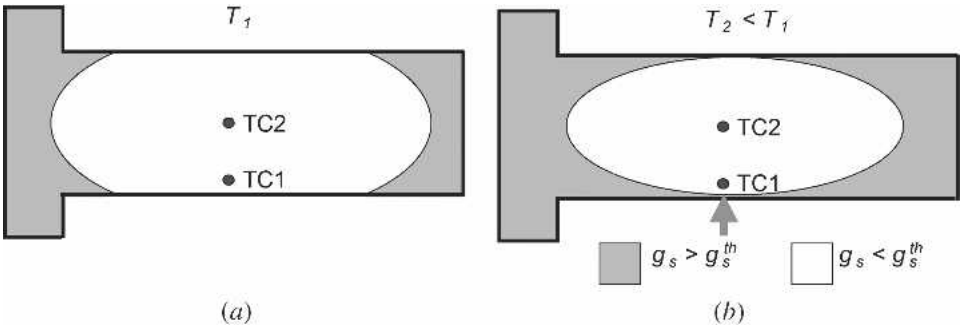

Fig. 3—Schematic view of the development of a coherent structure in the mushy zone close to the bottom of the mold at (*a*) high temperatures and (*b*) low temperatures. Two thermocouples are placed at the positions indicated by the labels TC1 and TC2. The arrow in (*b*) indicates the weakest position of the coherent solid structure at the moment when displacement of the moving block begins. This position is located at the bottom of the sample. g_s^{th} is the solid fraction at onset of contraction. The thickness of the layer where $g_s > g_s^{th}$, close to the position of the arrow in (*b*), is not measured, but this thickness is believed to be comparable to the size of dendritic arms.

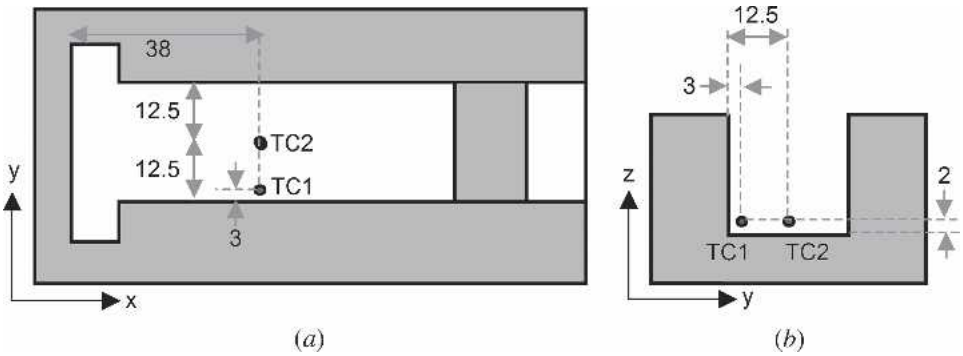

Fig. 4—The casting mold and the position of thermocouples, seen (*a*) from the top and (*b*) from the end. Dimensions are given in mm.

of both pure Al (99.99 wt pct) and pure Zn (99.99 wt pct). The reproducibility of the calibrations indicated an accuracy of ±1 °C in the temperature measurements.

The displacement of the moving block was measured by a linear RPD Electronics DCTH100 displacement sensor. The displacement measurements had an accuracy of ±2 μm. The linear solidification contraction,[11] d_{LSC}, and the expansion due to gas evolution, d_{exp}, are given by

$$d_{LSC} = \frac{l_0 + \Delta l_{exp} - l_f}{l_0} \cdot 100 \text{ pct} \quad [1]$$

and

$$d_{exp} = \frac{\Delta l_{exp}}{l_0} \cdot 100 \text{ pct} \quad [2]$$

where l_0 = the initial length of the sample and Δl_{exp} = the expansion of the casting before the onset of contraction (*i.e.,* the increase in linear dimension in the horizontal plane of the sample due to gas evolution at temperatures above T^{th}). l_f is the length of the sample when the temperature measured by thermocouple TC1 in Figure 4 reaches the nonequilibrium solidus. The temperature of nonequilibrium solidus is defined as the temperature of the lowest possible eutectic in the alloy.

When the solidus is reached at the position of thermocouple TC1, parts of the sample, which are close to the mold wall, have been fully solid for a short time, while the central part of the sample is still mushy. Because the geometric design of the mold thus might influence the contraction of the solidifying sample, d_{LSC} cannot be regarded as a fundamental measure of the contraction of the mushy zone.

It has been previously shown that the temperature at the onset of contraction is not affected by the friction forces existing between the moving block, the mold, and the sample, whereas the value of the thermal contraction may vary.[11] The choice of graphite as the mold material is stipulated by its very low friction and thermal expansion coefficients that minimize the effects of friction and mold thermal expansion on the measured parameters, especially on thermal contraction and expansion.

The compositions of the tested alloys are given in Table I. Experiments were carried out both with and without addition of an Al-5 wt pct Ti-1 wt pct B grain refiner rod. The added grain refiner increased the Ti concentration in the sample by 120 to 130 ppm compared to the original Ti concentration given in Table I. Experiments were also performed with Sr modification of the A356 alloy. The Sr concentration in the melt in these experiments was 123 to 126 ppm. Some experiments were carried out with additions of alloying elements, increasing the concentration of the alloying elements by 1 wt pct compared to the data given in Table I.

The melt temperature was 720 °C, and the melt was kept in the furnace at this temperature while being exposed to an

Table I. Chemical Compositions of the Alloys

Alloy	Cu	Si	Mg	Zn	Fe	Cr	Mn	Ti
A356	<0.001	7.05	0.29	0.0048	0.083	<0.001	<0.01	0.10
AA2024	4.00	0.08	1.48	0.005	0.15	0.007	0.37	0.004
AA6061	0.22	0.50	0.94	0.015	0.12	0.076	<0.01	0.005
AA7075	1.84	0.06	2.45	5.53	0.11	0.19	<0.01	0.005
A1–4 wt pct Cu	3.82	0.01	<0.01	<0.001	<0.01	<0.001	<0.01	<0.001

All data are given for unrefined alloys and in wt pct.

inert Ar atmosphere for approximately 30 minutes before casting. Grain refiner was added to the melt 10 minutes before casting.

III. DETERMINATION OF THE MACROSCOPIC THERMAL STRAIN

The constitutive equation for macroscopic thermal strain in the mushy zone was established by combining experimental data with thermomechanical modeling of the mushy zone. This is thoroughly outlined in Reference 9, and only the main aspects of this modeling work are repeated here. The volume-averaged displacement vector, $\boldsymbol{u}$, of the solid coherent structure in the experimental sample can be related to a solid strain tensor ($\varepsilon_{\mathbf{s}}$) by

$$\varepsilon_s = \frac{1}{2}\left(\nabla u_s + (\nabla u_s)^T\right) = \varepsilon_s^e + \varepsilon_s^p + \varepsilon_s^{th} \qquad [3]$$

where $\varepsilon_s{}^e$, $\varepsilon_s{}^p$, and $\varepsilon_s{}^{th}$ represent the solid elastic-strain tensor, the solid viscoplastic-strain tensor, and the solid thermal-strain tensor, respectively. In the experiment, the displacement of the sample boundary at the moving block is measured as a function of time, and this quantity was in Reference 9 related to the driving force for the thermally induced deformations ($\varepsilon_s{}^{th}$) by combining experimental results with thermomechanical simulations of the experiments.

With reference to Figure 4, the measured displacement of the moving block corresponds to the displacement in the x-direction (*i.e.,* u_x). The calculated quantity d_{LSC} thus corresponds to u_x at the position of the sample boundary at the moving block when the solidus temperature is reached by thermocouple TC1.

The constitutive equation that relates the macroscopic thermal strain rate, $\dot{\varepsilon}_s^{th}$, to the solid fraction and temperature is given by:

$$\dot{\varepsilon}_s^{th} = \frac{1}{3}\psi(g_s)\beta_T\dot{T}\,\mathbf{I} \quad \text{with}$$
$$\psi(g_s) = \begin{cases} 0 & \text{for } g_s \le g_s^{th} \\ \left(\dfrac{g_s - g_s^{th}}{1 - g_s^{th}}\right)^n & \text{for } g_s > g_s^{th} \end{cases} \qquad [5]$$

where β_T, $\dot{T}$, $\mathbf{I}$, g_s, and n are the volumetric thermal expansion coefficient, the cooling rate, the identity tensor, the solid fraction, and a material parameter, respectively. The solid fraction dependent function $\psi(g_s)$ takes into account that no thermal strain is transmitted through the mushy zone at low solid fraction (*i.e.,* at $g_s < g_s{}^{th}$). Macroscopic thermal strain in the mushy zone will tend toward thermal strain in fully solid as the solid fraction tends toward 1, and this is taken into account in Eq. [4] by the fact that $\psi(g_s) = 1$ for fully solid (*i.e.,* $\psi(g_s) = 1$ for $g_s = 1$). The material parameter n in Eq. [4] must be greater than or equal to 0 to make the function $\psi(g_s)$ increase from 0 at $g_s = g_s{}^{th}$ to unity for fully solid.[9] The volumetric thermal expansion coefficient, β_T, was taken in accordance with literature data.[15]

To determine the material parameter n in Eq. [4], the conservation equations for mass, momentum, and energy have been solved in a solution domain reflecting the experimental setup.[9] In this model, time-dependent heat transfer coefficients are tuned to fit the computed temperatures to the measured temperatures, and n is tuned to obtain a calculated displacement of the alloy at the moving block interface as close as possible to the experimentally determined displacement of the moving block.*

*It should be noted that the simulations of the experiment were carried out in a 3D solution domain. The 3D contraction of the solid part of the mushy zone is therefore taken into account. The contraction of the solid part of the mushy zone in the vertical direction will influence the deformation of the sample, but the solid fraction at onset of contraction, which is the most important parameter calculated in the paper, is not influenced by the contraction in the vertical direction.

IV. RESULTS

A. *Data Analysis*

As a typical example, measured temperatures and displacement for the alloy AA6061 are given in Figure 5. In this figure the vertical dashed line represents the moment when the displacement of the moving block shifts from expansion to contraction. Calculation of $g_s{}^{th}$ is based on the temperature measured by the thermocouple labeled TC1 at the time indicated by the dashed line.

Based on uncertainty in the calculated temperature gradients, the experimental margin in temperatures at the position of the arrow in Figure 3 was estimated to ±3 °C. For most experiments the change of displacement direction of the moving block occurred instantaneously, but for some experiments it took place over a temperature interval of up to 5 °C. All these uncertainties decrease the accuracy in determining the temperature at the onset of contraction and thus in the calculated $g_s{}^{th}$.

The uncertainty in linear solidification contraction, as well as expansion, is for each alloy defined as the standard

deviation from three or four experiments. The instrumental error of the displacement sensor was small compared to this experimental error.

B. *Thermal Strain*

Figure 6 shows an example of simulated and measured temperatures for the alloy A356. The time interval when the bottom center of the sample is mushy is of most interest, and this time interval is enlarged in the right part of this figure. It is seen from this figure that the differences between measured and calculated temperatures are within ±2 °C when the bottom center of the sample is mushy.

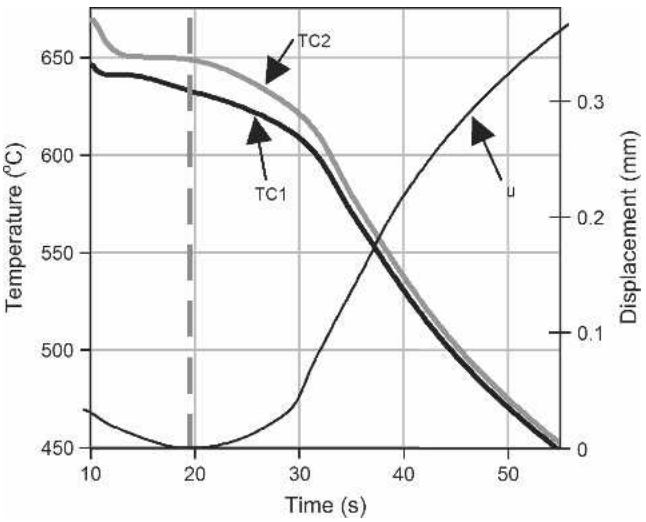

Fig. 5—Temperatures and displacement for the alloy AA6061. TC1 and TC2 are thermocouples with positions as defined in Figure 4, and u denotes the displacement of the moving block. The vertical dashed line indicates the moment when the displacement of the moving block shifts from expansion to contraction.

Simulations of thermally induced deformation were also performed for all the tested alloys, and the material parameter n in Eq. [4] was tuned to fit calculated displacement to measured displacement. As a typical example, calculated and measured displacement for the alloy A356 are shown in Figure 7. The experimental displacement in the time interval up to 16 seconds is a result of expansion of the mushy zone due to gas evolution. This effect has not been taken into account in the calculations. There is reasonably good correlation between calculated and measured data in the interval between 15 and 32 seconds when the bottom center of the sample is still mushy, while the calculations underestimate the contraction after about 29 seconds. This discrepancy is further discussed in Section V.

Measured and calculated results are given in Table II. The solid fractions at the onset of contraction, g_s^{th}, for the tested alloys are also plotted in Figure 8. As seen from this figure and Table II, contraction starts at high solid fractions, and g_s^{th} values for the tested alloys are in the range from 0.63 to 0.94. Ranking of grain refined alloys shows that g_s^{th} is highest for AA6061, and then A356, AA2024, and AA7075 when listed from highest to lowest g_s^{th}. Grain refinement as well as Sr modification of the A356 alloy increases g_s^{th}. It is also seen that additional alloying with Mg, Cu, and Zn decreases g_s^{th}.

It is seen from Table II that the linear solidification contraction, d_{LSC}, is in the range 0.09 pct to 0.59 pct. The alloys AA2024, AA6061, and AA7075 have much higher d_{LSC} than the alloys A356 and Al-4 wt pct Cu. The alloys with highest d_{LSC} also have the largest interval between g_s^{th} and $g_s = 1$, which means that largest contractions are observed when the contraction starts at relative low solid fractions.

The accuracy of determining g_s^{th} is within ±0.03 for all alloys except the A356-based alloys, where the accuracy in g_s^{th} is within ±0.1. This significant error is a result of the solidification path, because g_s^{th} for the A356-based alloys is in a range where g_s is strongly dependent on the temper-

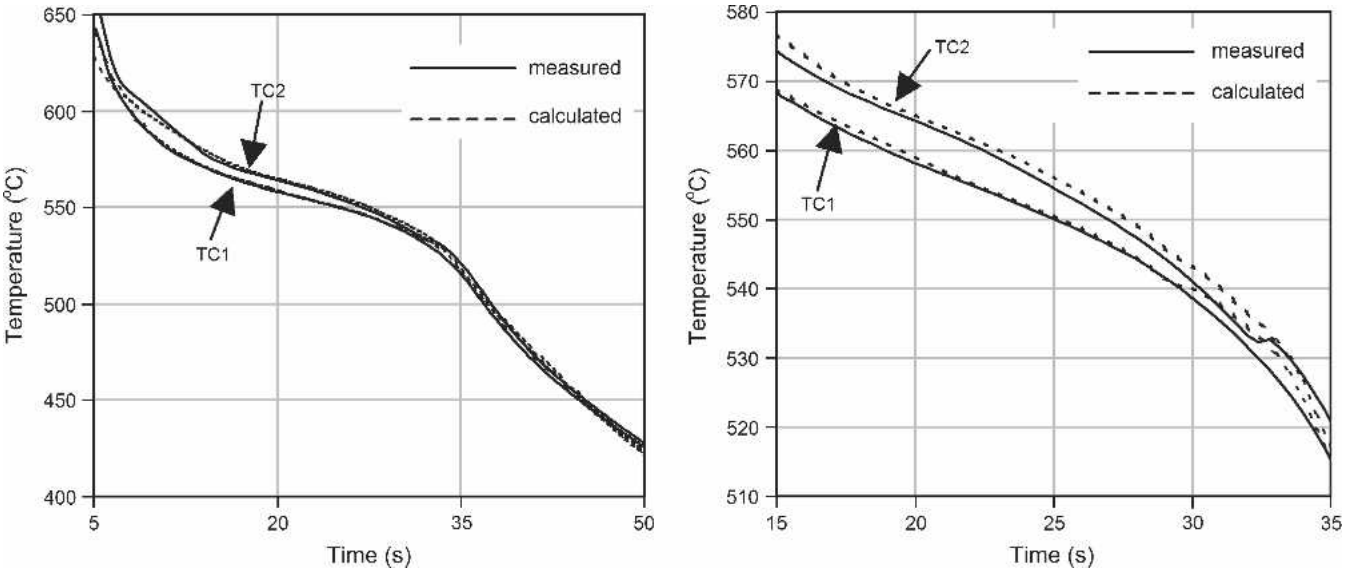

Fig. 6—Comparison of experimentally measured and calculated temperatures for unrefined A356. TC1 and TC2 are thermocouples with position as indicated in Figure 4. The right figure shows the most interesting time interval in which the bottom center of the sample is mushy.

ature (*i.e.,* small variations in temperature give large variations in g_s). The absolute value of the experimental error in d_{LSC} is within ±0.05 for the AA7075-based alloys, ±0.03 for the AA2024- and A356-based alloys, and ±0.02 for the Al-4 wt pct Cu and the AA6061-based alloys, respectively. The experimental error in d_{exp} is within ±0.02 (absolute value) for all tested alloys. There is significant uncertainty in both d_{LSC} and d_{exp}, but the more important parameter g_s^{th} can be determined rather accurately.

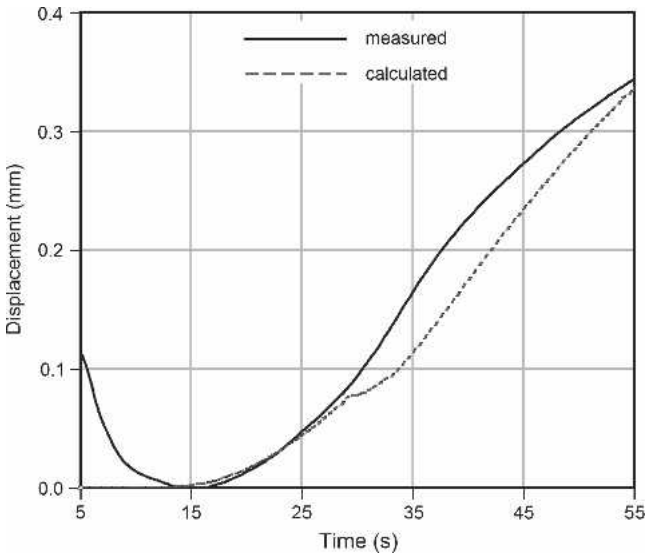

Fig. 7—Comparison between calculated and experimentally measured displacement of the moving block for unrefined A356. Positive displacement corresponds to contraction.

The macroscopic thermal strain in the mushy zone is quantified by the constitutive relation in Eq. [4] containing the parameters g_s^{th} and n. As seen from Table II, the material parameter $n = 0$ for all alloys except the alloy Al-4 wt pct Cu. When $n = 0$ it is seen from Eq. [4] that the function $\psi(g_s)$ becomes a step function—*i.e.,* $\psi(g_s) = 1$ for solid fractions equal to or higher than g_s^{th}. The function $\psi(g_s)$ is plotted in Figure 9 for some of the tested alloys. When the function $\psi(g_s)$ is a step function, the thermal strain in the mushy zone will instantly increase from 0 to the same value as thermal strain in fully solid once the solid fraction is equal to g_s^{th}.

C. *Metallographic Results*

The grain size, secondary dendrite arm spacing, and porosity were determined based on optical microscopy. The results are given in Table III, and micrographs from samples of both grain-refined and unrefined AA2024, AA6061, and AA7075 along with grain-refined A356 are given in Figures 10 through 16. The micrographs correspond to a position close to the bottom in the central part of the sample. Metallographic examination of unrefined A356 was reported in Reference 9.

Porosity is generally a result of the hydrogen amount and hindered feeding. For industrial castings, the experiments are designed to obtain good liquid feeding, resulting in porosity levels usually considerably lower than 1 pct. Due to poor melt feeding after the onset of contraction in the experiments in this work, the porosity is expected to be high. Structure examination of the samples shows that the porosity is indeed considerable. The large, black areas in some of the micrographs in Figures 10 through 16 are

Table II. Measured and Calculated Results. Reported Data are the Cooling Rate, Q, Liquidus Temperature, $T_{liquidus}$, Solidus Temperature, $T_{solidus}$, Temperature Measured by Thermocouple TC1 when the Contraction Started, T_{TC1}, Temperature at Onset of Contraction, T^{th}, Solid Fraction at Onset of Contraction, g_s^{th}, Measured Displacement of the Moving Block from the Start of the Experiment until the Solidus is Reached, $l_0 - l_f$, Measured Displacement due to Expansion of the Mushy Zone, Δl_{exp}, Linear Solidification Contraction, d_{LSC}, Expansion Prior to Onset of Contraction, d_{exp}, and Material Parameter n

Alloy*	Q [°C/s]	$T_{liquidus}$ [°C]	$T_{solidus}$ [°C]	T_{TC1} [°C]	T^{th} [°C]	g_s^{th}	$l_0 - l_f$ [mm]	Δl_{exp} [mm]	d_{LSC} [Pct]	d_{exp} [Pct]	n in Eq. [4]
A356	3.4	616.5	537.8	569.8	560.8	0.88	0.067	0.054	0.17	0.08	0
A356+GR	3.3	616.5	537.8	569.1	560.1	0.89	0.041	0.058	0.14	0.08	0
A356+125 ppm Sr	3.0	616.5	537.8	566.1	557.1	0.92	0.030	0.036	0.09	0.05	0
A356+1 wt pct Si	2.2	608.9	544.1	569.4	560.4	0.94	0.041	0.048	0.13	0.07	0
AA2024	4.4	641.0	453.6	601.9	592.9	0.75	0.274	0.038	0.45	0.05	0
AA2024+GR	5.5	641.0	453.6	581.7	572.7	0.82	0.232	0.044	0.39	0.06	0
AA2024+1 wt pct Cu	4.3	638.0	453.0	593.0	584.0	0.74	0.323	0.042	0.52	0.06	0
AA2024+1 wt pct Mg	3.8	635.1	453.6	597.7	588.7	0.69	0.334	0.039	0.53	0.06	0
AA6061	4.5	652.0	495.3	631.9	622.8	0.87	0.262	0.022	0.41	0.03	0
AA6061+GR	4.9	652.0	495.3	617.6	608.6	0.92	0.188	0.043	0.33	0.06	0
AA6061+1 wt pct Mg	4.4	646.8	491.3	616.5	607.5	0.85	0.243	0.037	0.40	0.05	0
AA7075	3.7	633.4	470.0	599.3	590.3	0.73	0.237	0.036	0.39	0.05	0
AA7075+GR	4.4	633.4	470.0	586.6	577.6	0.79	0.344	0.047	0.56	0.07	0
AA7075+1 wt pct Zn	3.6	631.8	473.1	601.7	592.7	0.69	0.347	0.035	0.55	0.05	0
AA7075+1 wt pct Mg	3.5	628.0	467.0	601.1	592.1	0.63	0.383	0.027	0.59	0.04	0
AA7075+1 wt pct Cu	3.5	630.6	472.2	600.2	591.2	0.66	0.377	0.031	0.58	0.04	0
AA7075+1 wt pct Si	3.4	628.2	431.7	589.6	580.6	0.68	0.379	0.037	0.59	0.05	0
Al-4 wt pct Cu	5.6	650.4	548.0	623.5	605.8	0.84	0.166		0.22		0.1

*Some of the tested alloys are based on the commercial alloys specified in Table I but with additional alloying elements. In these cases the concentration of the specified alloying element is 1 wt pct higher than in the base material. GR, grain-refined alloy.

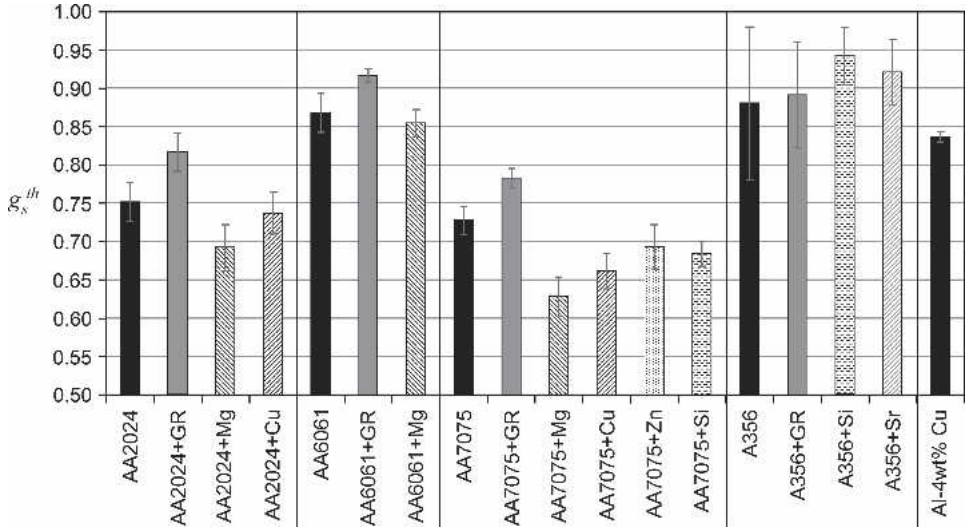

Fig. 8—Solid fraction at the onset of contraction, g_s^{th}, for the tested alloys.

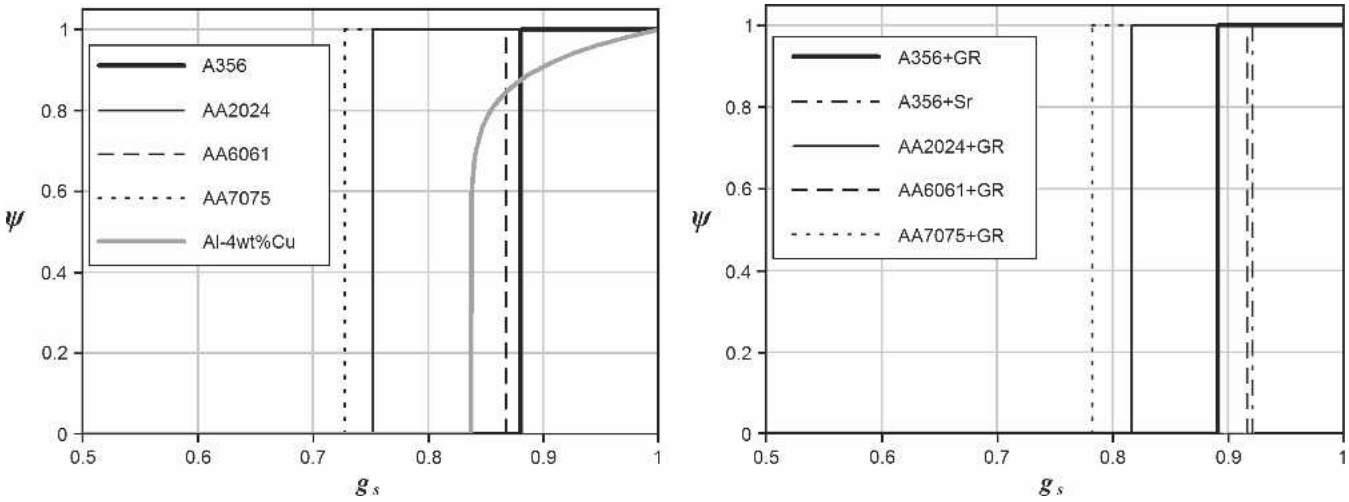

Fig. 9—The function $\psi(g_s)$ for the pure commercial alloys (left) and for grain-refined and Sr-modified alloys (right).

Table III. Grain Size, Secondary Dendrite Arm Spacing (DAS), and Porosity for the Tested Alloys

Alloy	Grain Refinement	Grain Size (mm)	DAS (μm)	Porosity (Pct)
A356	Yes	0.4 ± 0.3	20 ± 10	2.1 ± 0.6
AA2024	No	0.4 ± 0.3	30 ± 10	2.0 ± 0.8
AA2024	Yes	0.08 ± 0.04	25 ± 10	2.8 ± 0.3
AA6061	No	0.8 ± 0.6	45 ± 10	1.4 ± 0.3
AA6061	Yes	0.15 ± 0.05	45 ± 10	0.4 ± 0.2
AA7075	No	1.5 ± 1	30 ± 5	3.4 ± 1.3
AA7075	Yes	0.15 ± 0.05	30 ± 10	1.1 ± 0.5

pores. The high porosity levels reported in Table III correspond to porosity levels predicted by M'Hamdi *et al.*[13] Grain refinement reduces the porosity in the alloys AA6061 and AA7075, while the porosity is increased when the alloy AA2024 is grain refined.

Grain refinement reduced the grain size considerably for all the tested alloys, but grain refinement did not have any significant influence on the dendrite arm spacing.

V. DISCUSSION

Previously we showed that the solid fraction at the onset of contraction increases with increasing cooling rate.[9] In this work, $g_s^{th} = 0.84$ for the alloy Al-4 wt pct Cu at a cooling rate of 5.6 °C/s. This is consistent with previously reported results for the same alloy, where $g_s^{th} = 0.80$ and 0.89 at cooling rates of 3.5 °C/s and 8.9 °C/s, respectively.[9] Compared to previously reported data,[9] g_s^{th} for the alloy A356 also increases with increasing cooling rate.

Grain refinement increased g_s^{th} for all the tested alloys, and this is believed to reflect that small grains coalesce at higher solid fractions than larger grains. The onset of contraction is delayed when the alloys are grain refined.

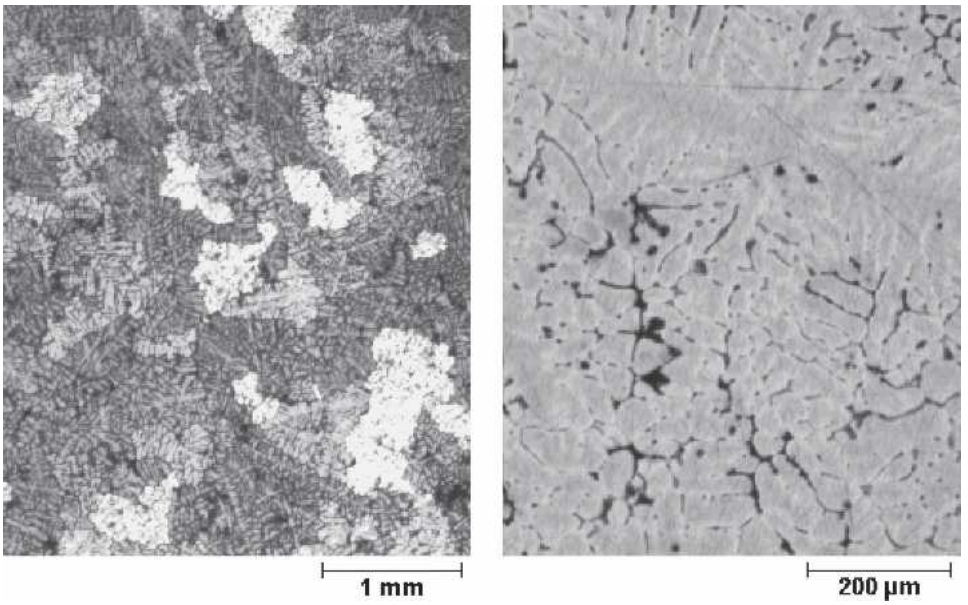

Fig. 10—Microstructure of unrefined AA2024 based on optical microscopy. Distributions of grains are shown in the left figure, dendrites in the right figure.

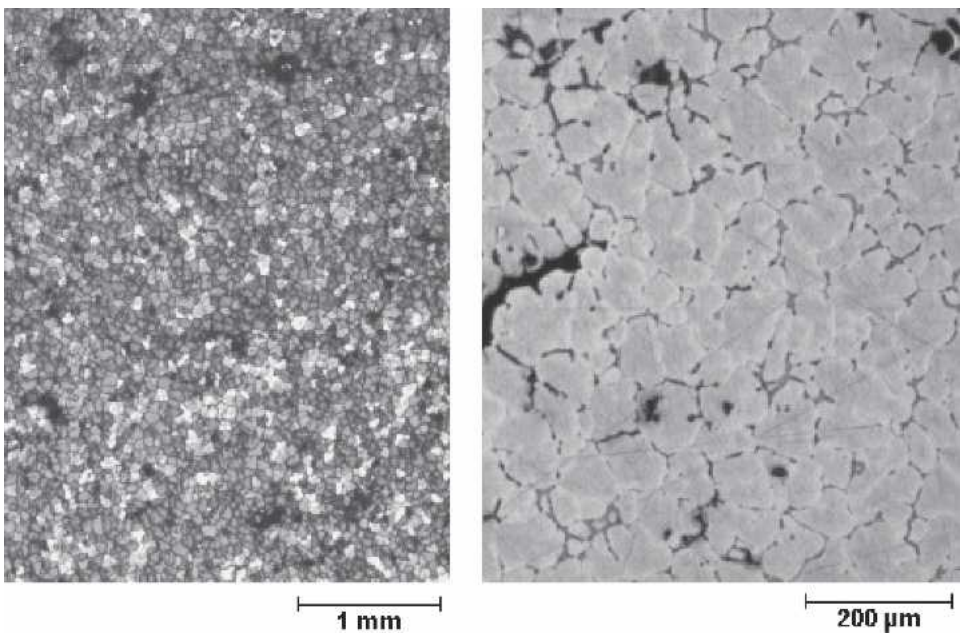

Fig. 11—Microstructure of grain-refined AA2024 based on optical microscopy. Distributions of grains are shown in the left figure, dendrites in the right figure.

Grain refinement decreases T^{th}, and thus the temperature interval between T^{th} and the nonequilibrium solidus also decreases. It is therefore reasonable to suggest that grain refinement will decrease d_{LSC}, which is observed in the experiments for most of the tested alloys. However, grain refinement increases d_{LSC} significantly for the AA7075 alloy. Similar results were reported by Novikov[10] upon adding small amounts of Mn and/or Zr to Al-Zn-Mg alloys. The reason for such behavior is unclear and requires further investigation.

The implications of the reported results for the development of hot tearing in aluminum alloys have been reported elsewhere.[10,12,16] The alloys with higher volume fraction solid at the onset of contraction and lesser total thermal contraction (strain) accumulated within the solidification range are less prone to hot tearing. Therefore, any means influencing these parameters (*e.g.,* grain refinement, additional alloying, gas saturation) are important for the susceptibility of the alloy to hot tearing. It is important here to note that the macroscopic thermal contraction is correlated to the macroscopic preshrinkage thermal expansion through the gas concentration in the melt. It has been reported elsewhere that alloys with the initially high concentration of dissolved gas and with subsequent high preshrinkage expansion during solidification are less prone to hot tearing.[10,12,17]

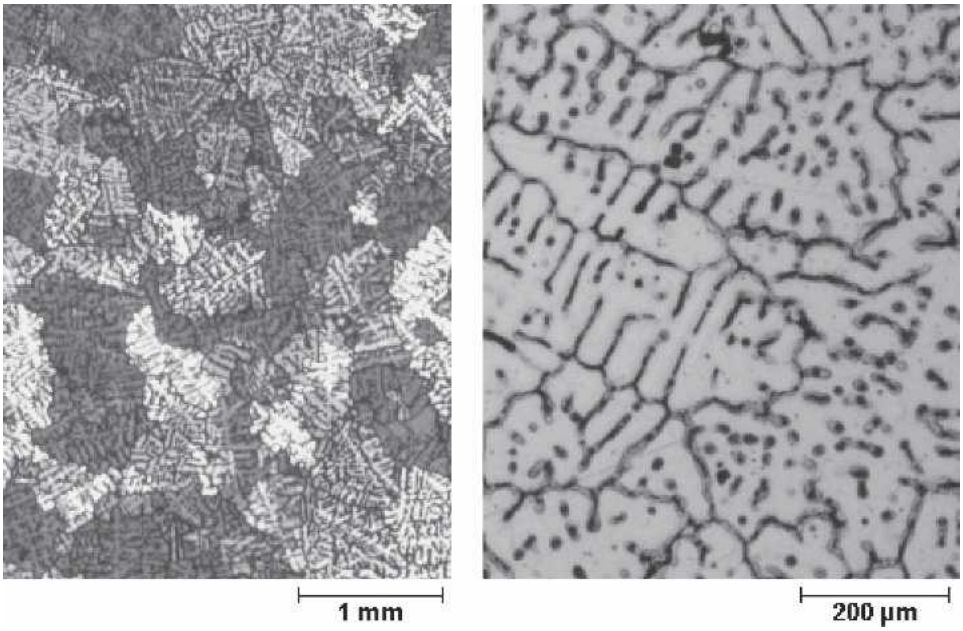

Fig. 12—Microstructure of unrefined AA6061 based on optical microscopy. Distributions of grains are shown in the left figure, dendrites in the right figure.

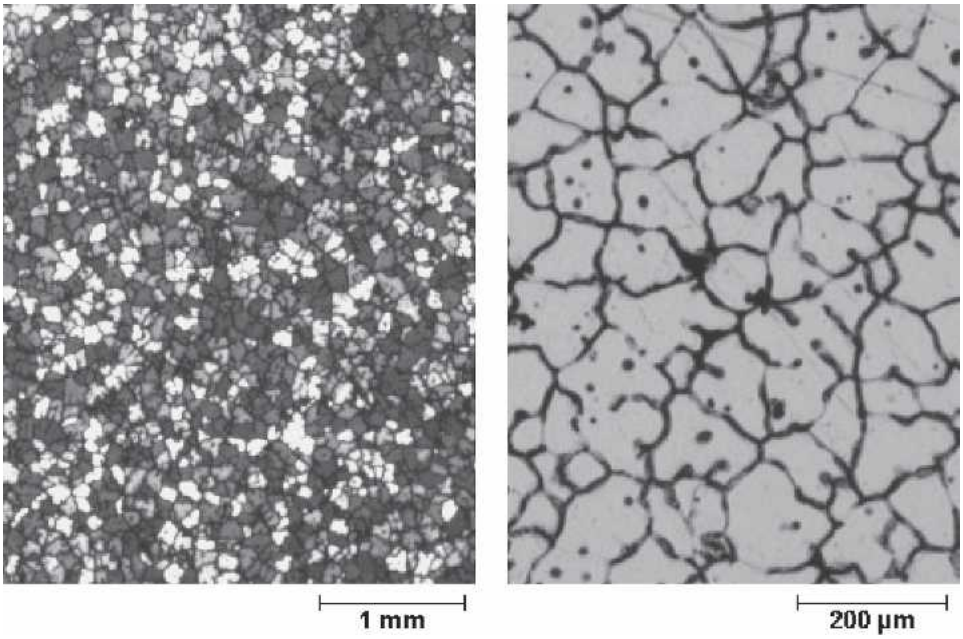

Fig. 13—Microstructure of grain-refined AA6061 based on optical microscopy. Distributions of grains are shown in the left figure, dendrites in the right figure.

Values for g_s^{th} were calculated based on the temperature at the onset of contraction, and the solid fraction as a function of temperature was calculated by the Alstruc model.[14] The Alstruc model is limited to maximum 1.3 wt pct Mg for Al-Cu-Mg alloys, and solid fraction *vs* temperature data could therefore not be calculated directly by the Alstruc model for the alloy AA2024, which contains 1.48 wt pct Mg. Solid fractions as a function of temperature for this alloy were calculated by extrapolation of data obtained for model alloys containing 1.0 and 1.3 wt pct Mg and otherwise same composition as that given for AA2024 in Table I. This extrapolation of data introduces an additional uncertainty in the calculated solid fractions for AA2024. However, this has to be rather small because there are small differences in solid fractions *vs* temperature for model alloys containing 1.0 and 1.3 wt pct Mg.

It is logical to suggest that the macroscopic thermal strain in the mushy zone cannot exceed the thermal strain in fully solid—*i.e.*, $\psi(g_s) \leq 1$ and $n \geq 0$ in Eq. [4]. Maximum thermal strain and maximum calculated contraction are then obtained when $n = 0$. It can be argued that it is physically impossible for the macroscopic thermal strain in the mushy zone to increase instantaneously when g_s reaches g_s^{th}, which is the case when $n = 0$. A more correct inter-

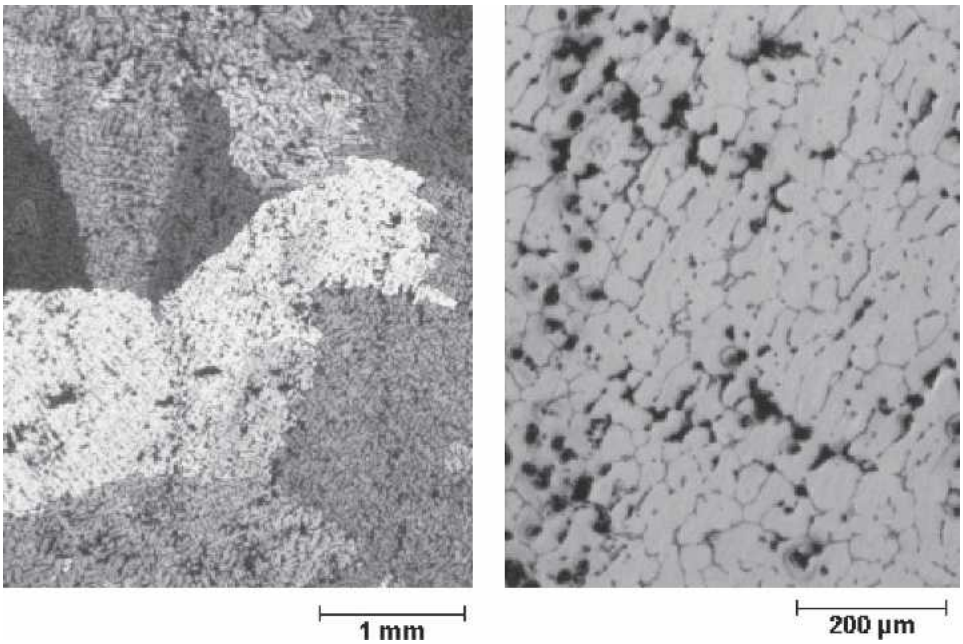

Fig. 14—Microstructure of unrefined AA7075 based on optical microscopy. Distributions of grains are shown in the left figure, dendrites in the right figure.

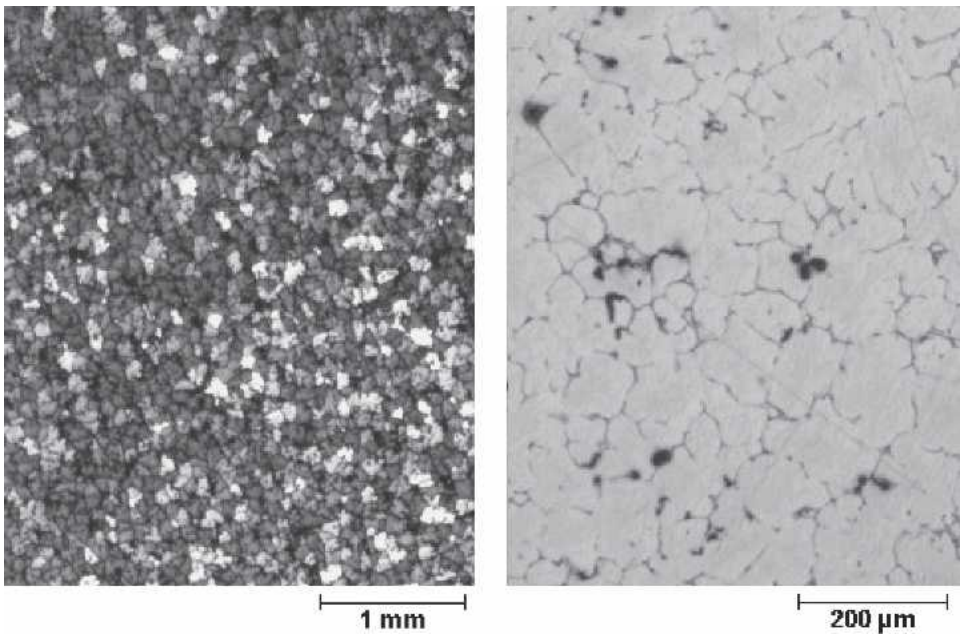

Fig. 15—Microstructure of grain-refined AA7075 based on optical microscopy. Distributions of grains are shown in the left figure, dendrites in the right figure.

pretation is that macroscopic thermal strain increases abruptly, but not instantaneously, and this requires n slightly above zero. From Figure 7 it is seen that the calculated displacement underestimates the measured displacement for the alloy A356 even though $n = 0$. A more accurate determination of the material parameter n requires a calculated temperature field that reproduces the physical temperature field, but there are uncertainties in the calculated temperatures because measured and calculated temperatures are compared in only two positions. Due to the uncertainties in the temperature field, setting the material parameter $n = 0$ is thus an acceptable approximation.

VI. CONCLUSIONS

The parameters in a model describing the constitutive relation for thermal strain in the mushy zone outlined elsewhere[9] have been determined for the commercial alloys A356, AA2024, AA6061, AA7075, and some model alloys. These parameters have been determined by combining

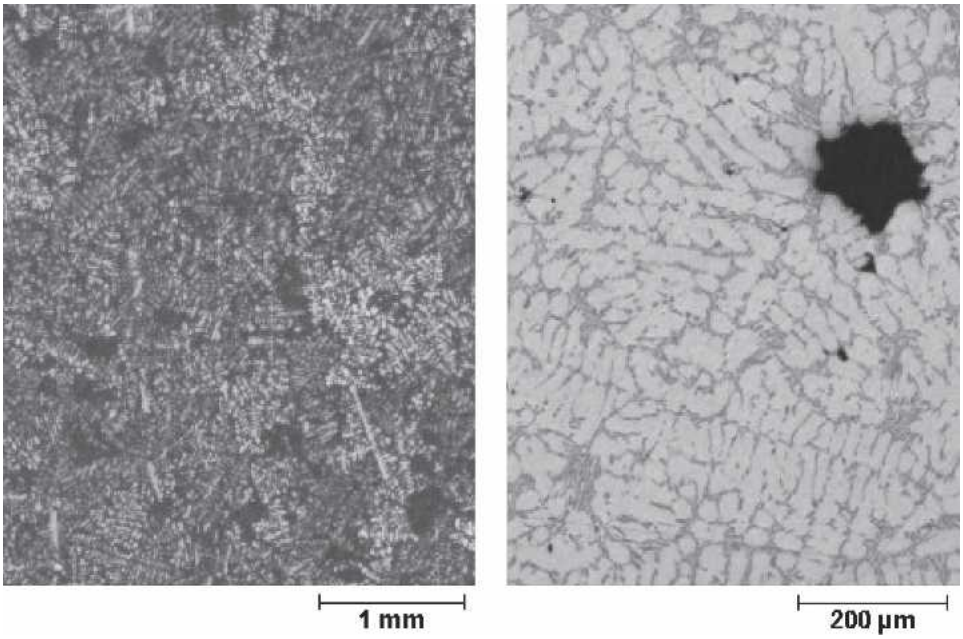

Fig. 16—Microstructure of grain-refined A356 based on optical microscopy. Distributions of grains are shown in the left figure, dendrites in the right figure.

experimentally measured deformation of the mushy zone with thermomechanical simulations of the experiment. The macroscopic thermal strain in the mushy zone is nonzero only for high solid fractions, and the limiting solid fractions when the macroscopic thermal strain becomes nonzero, g_s^{th}, are in the range from 0.63 to 0.94 for the tested alloys. Grain refinement increases g_s^{th}. For most of the tested alloys, the macroscopic thermal strain in the mushy zone increases almost instantly from 0 to the same level as in fully solidified material once the solid fraction becomes equal to g_s^{th}. Future work should be aimed at a better understanding of the mechanisms leading to changes in g_s^{th} when the concentrations of alloying elements are varied.

ACKNOWLEDGMENTS

The authors thank their SINTEF colleagues Dr. M. M'Hamdi, Dr. Ø. Nielsen, and Mr. M. Fleissner for useful comments, suggestions, and assistance. The work is Funded within the framework of the research program of the Netherlands Institute for Metals Research (NIMR) (www.nimr.nl), Project MC4.02135, and it has been carried out within the framework of the project NorLight Shaped Castings of Light Metals, with the following partners: Alcoa Automotive Castings, Scandinavian Casting Center ANS; Elkem Aluminium ANS; Fundo Wheels AS; Hydro Aluminium Metal Products; Hydro Magnesium; Netherlands Institute for Metals Research (NIMR); Norwegian University of Science and Technology (NTNU); and SINTEF (project responsible).

REFERENCES

1. J. Campbell: *Castings,* Butterworth Heinemann, Oxford, U.K., 1991.
2. M. Rappaz, J.-M. Drezet, and M. Gremaud: *Metall. Mater. Trans. A*, 1999, vol. 30A, pp. 449-55.
3. I. Farup and A. Mo: *Metall. Mater. Trans. A*, 2000, vol. 31A, pp. 1461-72.
4. Y.F. Guven and J.D. Hunt: *Cast Metals*, 1998, vol. 1, pp. 104-11.
5. M. M'Hamdi, A. Mo, and C.L. Martin: *Metall. Mater. Trans. A*, 2002, vol. 33A, pp. 2081-93.
6. J. Ni and C. Beckermann: *Metall. Trans. B*, 1991, vol. 22B, pp. 349-61.
7. P. Kolby, M. M'Hamdi, A. Mo, Ø. Nielsen, and P. Misic: *AFS Trans.*, 2002, vol. 110, pp. 367–74.
8. Y. Ju and L. Arnberg: *Int. J. Cast Met. Res.*, 2003, vol. 16, pp. 522-30.
9. A. Stangeland, A. Mo, Ø. Nielsen, D. Eskin, and M. M'Hamdi: *Metall. Mater. Trans. A*, 2004, vol. 35A, pp. 2903-15.
10. I.I. Novikov: *Goryachelomkost Tsvetnykh Metallov i Splavov*, Nauka, Moscow, 1966.
11. D. Eskine, J. Zuidema, Jr., and L. Katgerman: *Int. J. Cast Met. Res.*, 2002, vol. 14, pp. 217-24.
12. D.G. Eskin, Suyitno, J.F. Mooney, and L. Katgerman: *Metall. Mater. Trans. A*, 2004, vol. 35A, pp. 1325-35.
13. M. M'Hamdi, A. Pilipenko, and D. Eskin: *AFS Trans.*, 2003, vol. 111, pp. 333-40.
14. A.L. Dons, E.K. Jensen, Y. Langsrud, E. Trømborg, and S. Brusethaug: *Metall. Mater. Trans. A*, 1999, vol. 30A, pp. 2135-46.
15. *Aluminum and Aluminum Alloys*, ASM Specialty Handbook, J.R. Davis, ed., Materials Park, OH, ASM International, 1993.
16. A. Stangeland, A. Mo, M. M'Hamdi, D. Viano, and C. Davidson: *Metall. Mater. Trans. A*, 2006, vol. 37A, pp. 705–14.
17. R.S. Barnett, G. Kelly, and D.H. St. John: Light Metals (Metaux Legers) 2001: International Symposium on Light Metals, held at the 40th Annual Conference of Metallurgists of CIM (COM 2001). Toronto, Ontario, 26–29 Aug. 2001, pp. 491-500.